Supporting information

Electrochemically-grown Chloride-free Cu_2O Nanocubes Favorably Electroreduce CO_2 to Methane: The Interplay of Appropriate Electrochemical Protocol

Stefan Popović*[a,b], Mohammed Azeezulla Nazrulla[a], Primož Šket[c], Khaja Mohaideen Kamal[d], Blaž Likozar[d], Luka Suhadolnik[e], Luka Pavko[a], Angelja Kjara Surca[a], Marjan Bele[a], Nejc Hodnik*[a,b]

[a] Department of Materials Chemistry, National Institute of Chemistry, Hajdrihova 19, 1000 Ljubljana, Slovenia
[b] University of Nova Gorica, Vipavska 13, 5000 Nova Gorica, Slovenia
[c] Slovenian NMR Center, National Institute of Chemistry, Hajdrihova 19, 1000 Ljubljana, Slovenia
[d] Department of Catalysis and Chemical Reaction Engineering, National Institute of Chemistry, Hajdrihova 19, 1000 Ljubljana, Slovenia
[e] Department of Chemical and Pharmaceutical Sciences, University of Trieste, via L. Giorgieri 1, 34127 Trieste, Italy

Table of Contents

Supplementary note 1

Synthesis of Cu_2O nanocubes (Cu NCs) – floating method

10 mM copper sulfate-pentahydrate ($CuSO_4 \cdot 5H_2O$) (Sigma-Aldrich, 99%) without Cl^- contamination[1] was used as an electrochemical deposition solution. The standard three-electrode glass cell was used for the electrodeposition, which was boiled in Milli-Q water each time before deposition (Figure S1 A). Platinum rod and macro $Ag/AgCl_{3M\ KCl}$ served as counter and reference electrodes, respectively. Pre-cleaned glassy carbon plates were employed as a substrate for the Cu NCs synthesis. Before deposition, Teflon masks (dimensions of 25x25mm) with exact 1cm^2 opening were stuck with glassy carbon plates by copper foil tape to limit the surface area (Figure S2 B). Pulse-alternating method was employed between -0.3V vs. Ag/AgCl and open-circuit potential (OCP) with a total of 10 cycles for the synthesis of narrow-sized Cu NCs (Figure 1). 10 reductive pulses consisted of a first pulse of 2s and 9 consecutive pulses of 0.5s. The oxidative pulses in-between OCP were constant 30s for all 10 cycles. The completion of synthesis for one electrode was finished with an oxidative pulse. A magnetic stirring bar (5mm) was used to stir the deposition solution at a 500 rpm rate. After synthesis, the Teflon mask was removed and the electrode was thoroughly rinsed with Milli-Q water, followed by blow-drying with nitrogen.

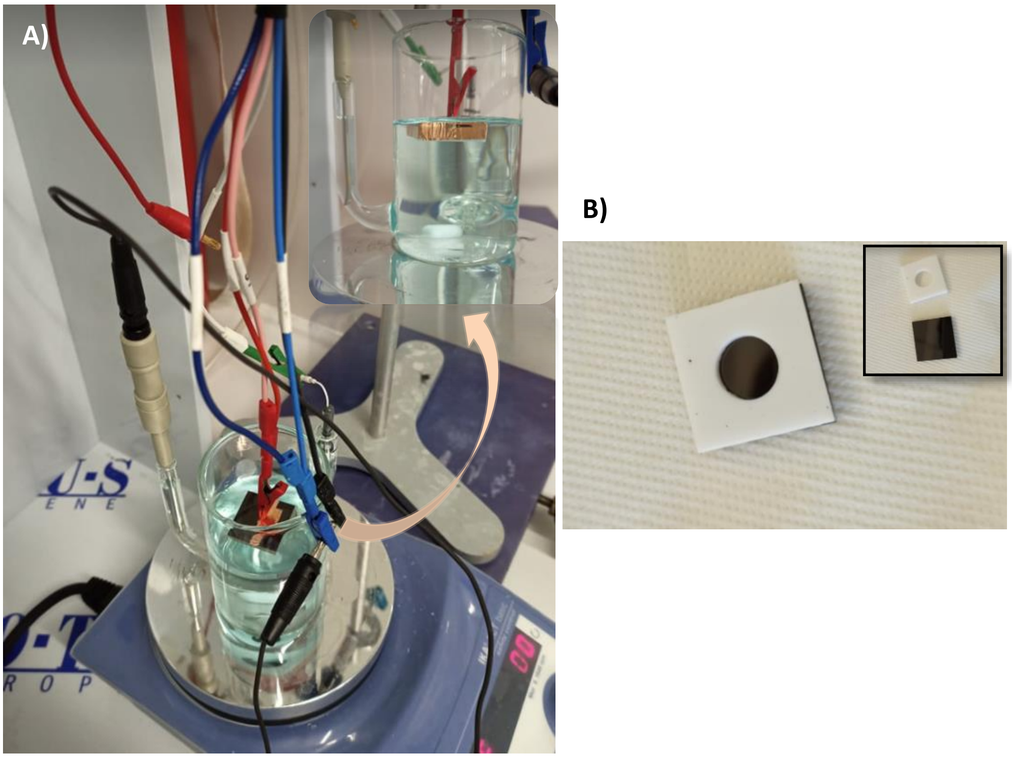

Figure S1. A) Standard three-electrode cell with 10 mM $CuSO_4$ solution bath and a working electrode in the »floating« position (inset). B) 25x25mm Teflon masks with exact 1cm^2 to limit geometrical surface area.

---

[1] Since it is commonly reported that macro Ag/AgCl might contaminate deposition solution during operation, electrodeposition has been done with the bridge setup (picture not depicted) and with the leak-free Ag/AgCl electrode. No observable differences were noticed.

Influence of the stirring rate of electrolyte

Electrodeposition is a rather complex process, where the synergy of numerous parameters plays a role in the final size, shape, morphology, and composition of the deposits. In the recent studies of the synthesis of Cu NCs, with abundant Cu(100) facets, a lot of effort has been made to achieve optimal and reproducible conditions for the synthesis.[1] The pulse-alternating method has been proposed as the perspective method to synthesize size-controlled Cu NCs. Tuning the reductive/oxidative duration of the pulses accompanied by the number of cycles, and the chemical composition of the bath has shown to mainly govern the synthesis of Cu NCs.[2] To the best of our knowledge, none of the studies addressed the stirring rate of electrolytes in the synthesis of shaped copper-based nanocatalysts. However, Lee et al.[3] pointed out that the diffusion rate of Cu ions influence the growth of microstructures receiving the different micro-shapes at different stirring rate. In the extensive review of nanofabrication of electrodeposits, Kondo et al. highlighted that the electrodeposition process is mass transfer-limited.[4] Since the pulse-alternating method has also been employed in our study, to produce Cu NCs catalyst, in the next section, we posit how the electrolyte stirring effect influences the shape in Cl^- -free electrodeposition bath.

To prove that diffusion plays a massive role in the synthesis of Cu NCs, firstly, we examined the selectivity of the deposit shape concerning the position of the working electrode when the electrolyte was not subjected to mixing. All experiments were conducted with the same electrochemical procedure (See Supplementary note 2) unless it is noted. Figure S2. A shows the two identical experiments where the working electrodes were in the »floating« position. The micrometer-sized deposits are produced in the absence of any particular trend. The reproducibility is poor, deposits are randomly shaped where some of them expressed certain facets but the process is rather not straightforward. Moreover, we investigated the shape and size of the electrodeposited when the working electrode (fully covered with Teflon tape) is immersed in the electrodeposition solution (Figure S3 B). The result is the formation of vaguely defined cubic shapes of approximately 450nm, with punctuated and truncated facets. Moreover, we observed the nonuniformity in coverage and the presence of copper micrometer-range agglomerates. These initial investigations shed a light on the importance of diffusion during the electrodeposition process.

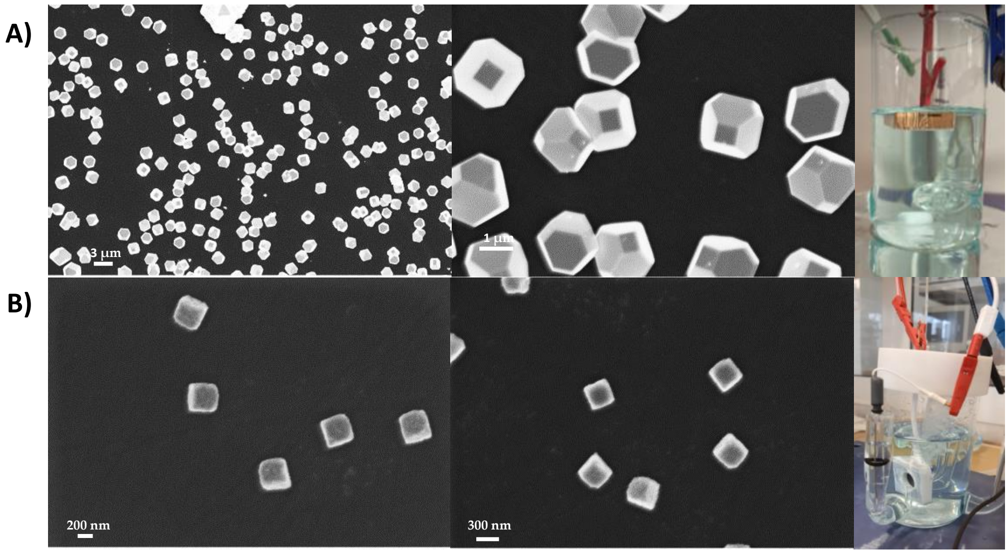

Figure S2. Set of two identical experiments of electrodeposition in 10 mM $CuSO_4$ solution without stirring (0 rpm) where the working electrode is in A) «floating«, and B) immersed position. The electrochemical procedure for all 4 experiments is the same. The pulse-alternating method is employed. In total 10 reductive cycles (first cycle 2s and rest 9 of 0,5s), with in-between oxidative pulses at OCP for the 30s.

The above initial investigations prompted a further study to examine the influence of diffusion on the synthesis of Cu NCs.There have been strong assertions that the composition of the electrodeposition bath, in particular, the optimal concentration of Cl- in the electrodeposition solution, plays a critical role in the electrochemical growth of Cu NCs. We posited that Cl^--free synthesis can be achieved with an appropriately optimized electrolyte stirring rate, whereby diffusion and electrodeposition kinetics are affected.. The electrochemical procedure for the synthesis of Cu NCs with a clear shape and narrow size is described in Supplementary note 2. The steps towards the optimized procedure consisted of the investigation of the stirring rate of a magnetic bar on the electrodeposited Cu NCs when the working electrode is in the »floating« position. Figure S4 shows the influence of the stirring rate on the shape of the Cu deposits. The three stirring rates of 500, 600, and 700 rpm were employed. Starting with the highest stirring rate of 700 rpm, we obtained particles of 700-800 with a shape that is irresistibly reminiscent of the tridiminished icosahedron. The particles' shape and size were uniform and covered all of the 1cm^2 geometrical area. The 600 rpm stirring rate, for the same electrodeposition procedure, produced a mixed state shape in the equal range of size. Apart from the same shape, we observed at 600 rpm, the existence of the dodecahedron-like shape. The cubes were not observed at a particular stirring rate. 500 rpm turned out to be the optimal stirring rate for the synthesis of Cu NCs, whose shape, reproducibility, and narrow size distribution are supported in Figures S5 and S6. Figure S5 represents high magnification SEM images of independent electrodeposition synthesis experiments confirming sharp-edge narrow-size Cu cubes. To further statistically prove the reproducibility of the synthesis of Cu NCs, we performed size-distribution analysis and loading determination from SEM images in ImageJ software. The three independent samples are taken and size-distribution analysis was done at the same magnification of 5000. The average particle size and loading from the three measurements are (515 ± 82) nm and 7%, respectively. In the main manuscript, the particle size will be denoted as »500nm« (Figure S6).

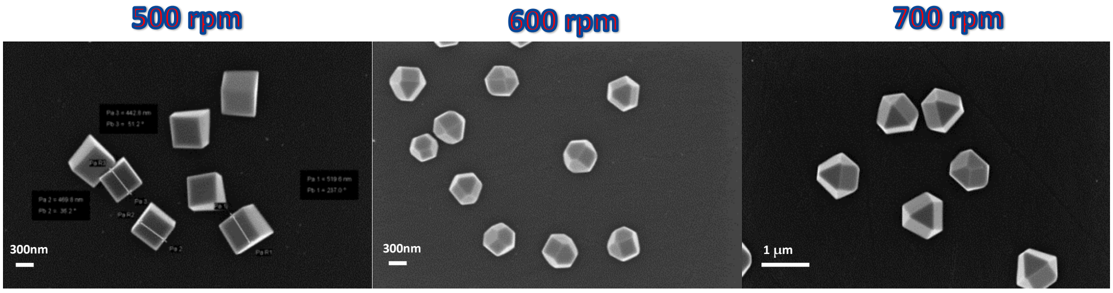

Figure S3. The influence of the stirring rate of electrolyte on the shape of copper nanoparticles. 500 rpm as the optimum rate to produce Cu NCs.

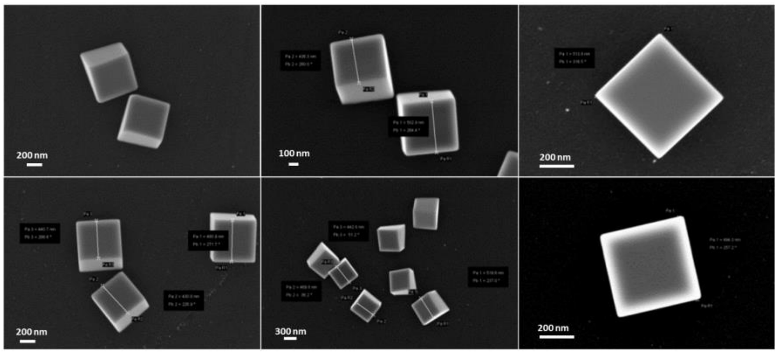

Figure S4. High magnification SEM images. The confirmation of the reproducibility of electrochemically-grown copper nanocubes (Cu NCs). Each SEM image corresponds to an independent electrodeposition experiment.

Sample	Size (nm)	Loading (%)
1	534 ± 77	7,4
2	520 ± 89	8,2
3	490 ± 80	5,4

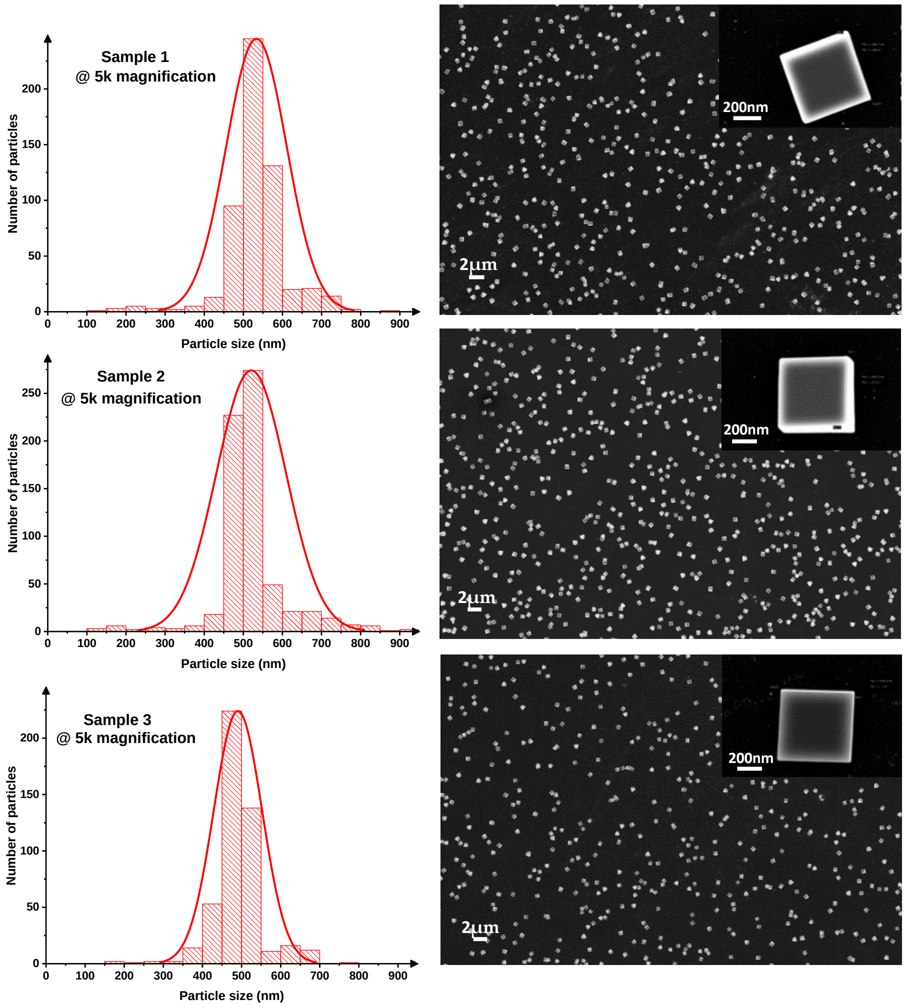

Figure S5. Tabulated averaged particle size and loading with corresponding size-distribution analysis with attached SEM pictures (at 5000 magnification) for three independent electrodeposition synthesis experiments.

Chloride effect

Since that Cl^- concentration is reported to have a drastic effect on the catalyst size, distribution, and coverage, we tried to synthesize Cu nanocubes in our electrochemical setup with the same electrochemical protocol and optimized stirring rate of 500rpm with the addition of Cl^- (Figure S2.). Grosse et. al[2] reported that the formation of sharp corner cubes can be achieved in a slightly different electrochemical protocol with optimal 5 mM KCl. We found the formation of imperfect cubes with coarsened edges and punctated facets with a wider range of size when we added 5 mM Cl^- in a 10 mM $CuSO_4$ electrodeposition bath. Figure S7 represents SEM images of three independent electrodeposition syntheses with Cl^- addition. The investigation of CO_2RR electrocatalytic activity/selectivity of Cl^- -containing Cu NCs is beyond the scope of this work, but Seunghwa et al.[5] showed that chloride-induced Cu_2O-Cu catalyst can produce C_2-C_4 species.

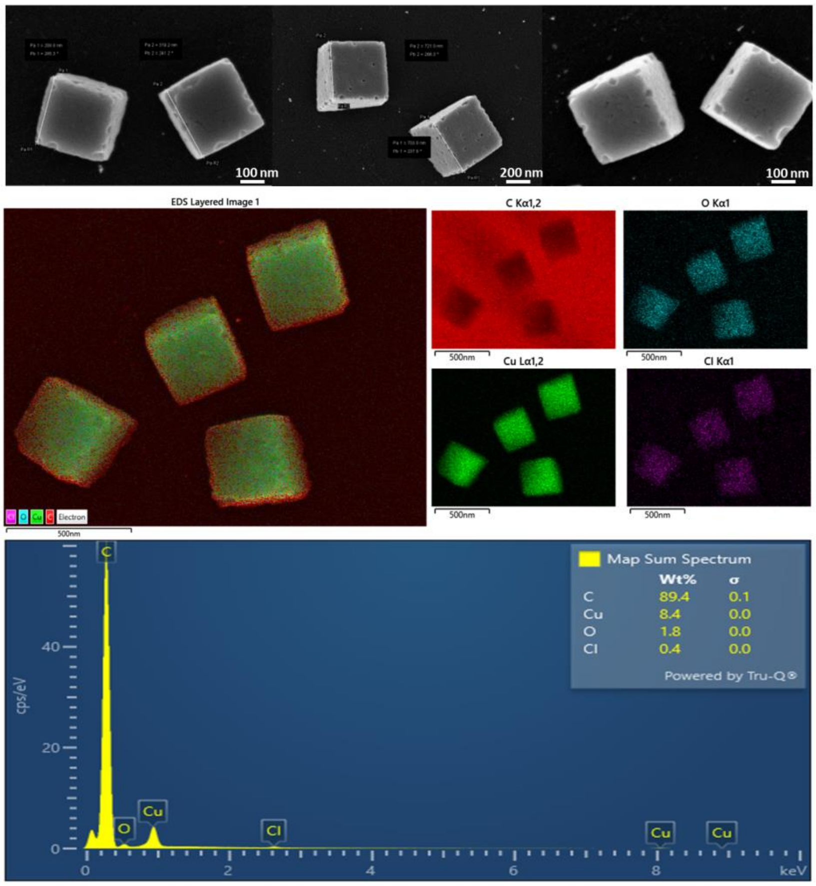

Figure S6. The influence of Cl^- addition on the electrodeposition synthesis of Cu nanocubes on a glassy carbon substrate. Coarsened Cu nanocubes with punctuated facets were observed in the electrodeposition bath of 10 mM $CuSO_4$ with the addition of 5mM Cl^-

Tuning electrochemical protocol – increased size of Cu NCs

In the already mentioned study, a group led by prof. Roldan Cuenya, the liquid-TEM technique confirmed that the cubes grow in layers when applying a reductive pulse. Namely, in an electrodeposition solution that contained 5mM KCl, they showed that by increasing the number of pulses, it is possible to manipulate the particle size. To apply the same approach in our electrochemical protocol (different from the one mentioned) in a Cl^- -free solution (stirring the solution at 500rpm), we did 3 types of experiments where we increased the number of cycles to 20, 30, and 50. In Figure S8 it can be seen that the particles in the range of 600 nm, 800 nm, and 1.2 μm were successfully synthesized, respectively for the stated number of cycles.

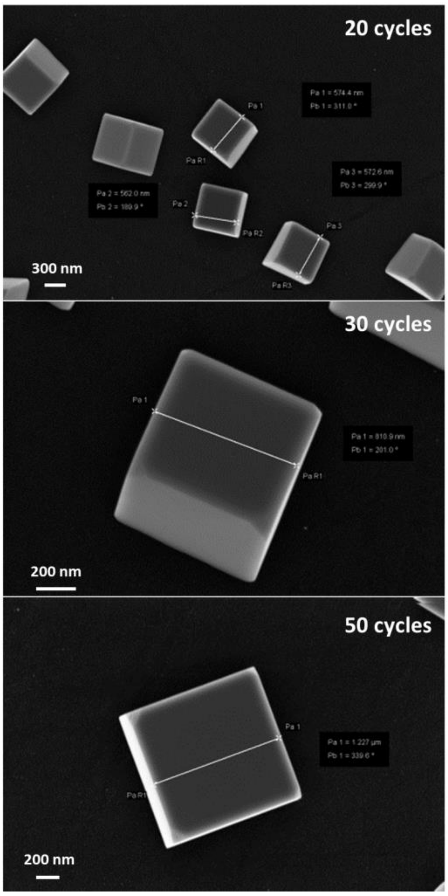

Figure S7. Gradual increase in the size of Cu NCs by increasing the number of cycles with the same electrochemical protocol described in the synthesis part. The size of Cu NCs are ranging from approximately 600 nm, 800 nm, and 1,2 μm for the 20, 30, and 50 cycles, respectively.

Supplementary note 2

XPS measurements of as-prepared Cu NCs

X-ray photoelectron spectroscopy (XPS) was performed with the Versa probe 3 AD (Phi, Chanhassen, US) using a monochromatic Al K_α X-ray source. A glassy carbon plate with electrodeposited copper nanocubes was attached to the XPS holder using conductive copper tape. For each measurement, spectra were acquired on a 1 x 1 mm analysis spot size with a charge neutralizer turned off. Survey spectra were measured at a pass energy of 224 eV and step of 0.8 eV, while high-resolution (HR) spectra were measured at a pass energy of 27 eV and step of 0.1 eV. For survey spectra, 10 sweeps were performed and for all the HR spectra measurements at least 15 sweeps were performed. The energy scale of XPS spectra and possible charging effect were corrected using the C 1s peak of carbon at binding energy (BE) of 284.8 eV. After the acquisition of the spectra, the data were processed with Tougaard background subtraction in Origin software. The accuracy of the binding energy scale is estimated to be 0.2 eV. High-resolution spectra for C 1s, O 1s, Cu 2p, as well as the X-ray excited Auger peak Cu LLM were analyzed.

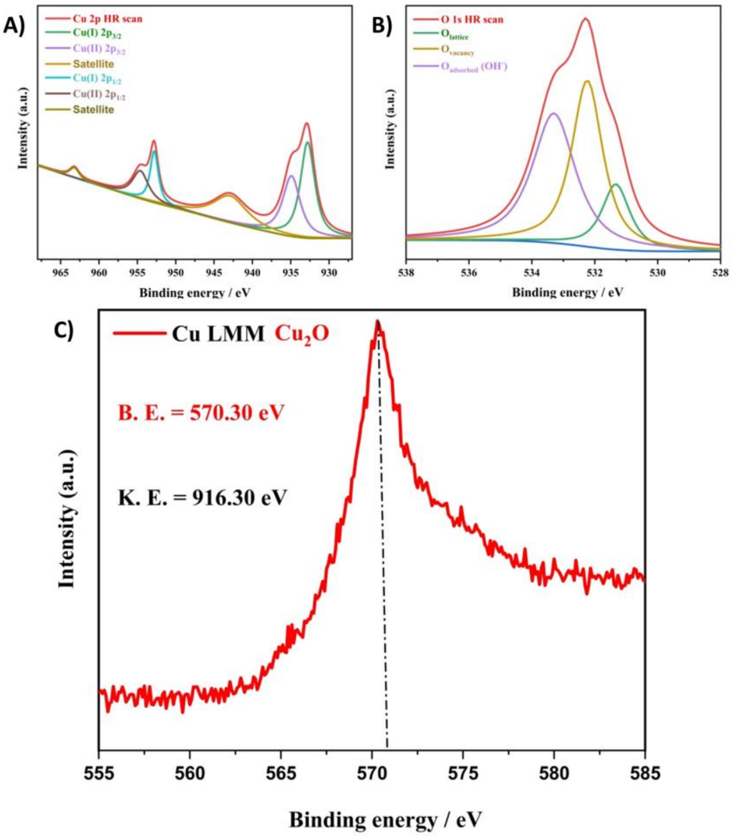

Figure S8. XPS measurements of as-prepared Cu NCs. A) Cu 2p region spectra with deconvoluted peaks. The satellite features at 933.5 and 943 eV correspond to the Cu(II) which we ascribed to partial near-surface oxidation of the already confirmed Cu_2O bulk structure. B) O1s high-resolution spectra with deconvoluted peaks of different origins of oxygen. C) Cu LMM XAES spectra with the peak at 570.30 eV binding energy.

Sputtering procedure

To remove the few top layers of the sample to examine the bulk surface of Cu NCs (Figure 2E, F), sputtering of the sample with Ar^+ was performed. Sputter time was 2 minutes at 1 kV over a 3 x 3 mm area with Zalar rotation turned on. Zalar rotation was turned on to eliminate the sample roughening and to sputter the sample more evenly. Right after sputtering HR spectra for C 1s, O 1s, Cu 2p, as well as the X-ray excited Auger peak Cu LLM were acquired and analyzed as described previously.

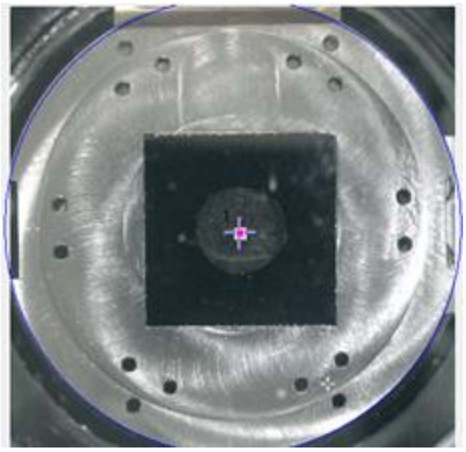

Figure S9. View of GC plate with as-prepared CuNCs at XPS with squared sputtered area

XRD measurements of as-prepared Cu NCs

Very slow scan X-ray diffraction (XRD was recorded on Bruker AXS diffractometer with Cu-Kα radiation (λ=1.5406 Å), 2θ angular range is from 25° to 90° with $2.78 \cdot 10^{-5}$ °/s (run time around 8h). In the absence of grazing incidence XRD, it is important to emphasize that with the usual scan rate of $3.39 \cdot 10^{-4}$ we were not able to observe the Cu_2O diffraction peaks (graph not depicted).

Raman measurements of as-prepared Cu NCs

Raman measurements were performed on a confocal Raman spectrometer WITec alpha 300 using a green laser excitation light of 532 nm. The spectra were measured with 100 scans using integration time IT = 1, 2, or 4 and laser power of 0.6 or 3.4 mW.

Supplementary note 3

The electrochemical custom-made cell configuration

The electrocatalytic measurements were performed in a custom-made sandwich-type cell.[6] The electrochemical custom-made sandwich-type cell for CO_2RR is composed of an anode and cathode compartments, separated by an anion-exchange membrane, Selemion AMV (AGC engineering Co.). The two compartments are made from poly(methylmethacrylate) also so-called plexiglass, and all components are designed to be removable for cleaning purposes. Before each experiment, all the parts of the electrochemical cell (PMMA material) were left for cleaning in a 30 wt% nitric acid bath for at least 30min. Afterward, all the parts were rinsed 3 times with Milli-Q water (18.2 MΩ·cm) and additionally ultrasonicated 3 times for 10 min in Milli-Q water to remove any residues. The cell is designed to maintain a parallel plate electrode geometry to ensure a uniform voltage field over the catalyst surface. A 1 mm OD Ag/AgCl leak-free reference electrode (Innovative Instruments) is employed as the reference electrode in the cathode chamber to monitor the working electrode potential. All voltages in the work are converted against an ideal reversible hydrogen electrode. The platinum foil (GoodFellow 99,95%, 25x25mm) is used as a counter electrode. Glassy-carbon plates (Type 2, Alfa Aesar, thickness 3mm) with a surface area of 2,5cm x 2,5 cm were used as a substrate for the working electrode. The geometric surface area for both of the electrodes was 1 cm^2. The cell is sealed by compressing the stack of the counter electrode, anode chamber, membrane, cathode chamber, and working electrode between two outer plates secured with bolts. O-rings are used to seal both compartments. To provide online GC measurements, Festo push-in fittings were employed to connect 1/8" tubing between the cell and a gas-chromatograph.

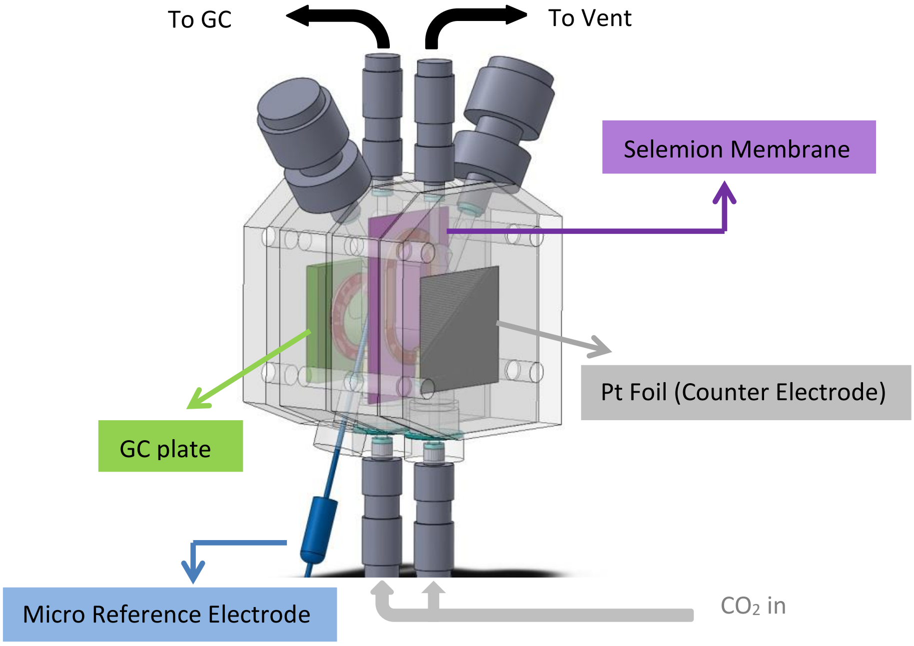

Figure S10. Schematic representation of the sandwich-type cell. The cell is made of two poly(methyl methacrylate) compartments with identical volumes separated by a membrane. Both sides are sparged with CO_2 with a controlled flow rate.

Supplementary note 4

Electrochemical surface area (ECSA) determination

Widely speaking, in the field of electrocatalysis, one of the most important parameters characterizing the surface of solid electrodes is the real surface area (RSA). The solid electrodes are usually rough, and their real area exceeds the geometric one, which serves as the figure of merit for current normalization and subsequent intrinsic activity comparison. The synonym which is mostly used in the electrocatalysis community for RSA is electrochemically active surface area (ECSA). Among the various methods of ECSA determination as hydrogen adsorption, surface oxide reduction, CO stripping and underpotential deposition of metals, one of the most popular methods for measuring the ECSAs in the CO_2RR community is the double-layer capacitance method.[7] The method is based on double-layer capacity voltammetric curves which are recorded in the double-layer region at various scan rates (in our case 20, 50, 100, 200, and 300 mV/s). Afterward, a plot of the anodic or cathodic current in the middle of the potential window versus the scan rate is constructed. The plot follows the expected linear behavior (in the absence of faradaic processes) of an ideal capacitor with scan rate (equation 4). The slope is equal for C_{dl}. The ECSA is calculated by referring the obtained capacity to the reference value of capacity per unit area $C_{dl\ ref.}$ (equation 5).

$$i_a = \frac{dQ}{dt} = \left(\frac{dQ}{dE}\right) \cdot \left(\frac{dE}{dt}\right) = C_{dl} v \quad \text{(equation 4)}$$

$$ECSA = \frac{C_{dl}}{C_{dl\,ref.}} \quad \text{(equation 5)}$$

The $C_{dl\ ref.}$ is most of the time taken from the literature and it can typically vary from 20 to 40 $\mu F/cm^2$.[8] However, in our study, we referred capacity to as the reference value of blank glassy carbon capacity measured under the same conditions as for the as-prepared Cu NCs. The value of $C_{dl\ ref.}$ used for all the samples is 30,96 $\mu F/cm^2$. Tables 1 and 2 show cell currents, ECSA-normalized currents, and ECSA-normalized partial current density for methane for Cu NCs-OCP200 and Cu NCs-OCP400, respectively. Figure S14 and S15 represent the ECSA determination method with $i_a = f(v)$ plots and corresponding cyclic voltammograms for Cu NCs-OCP200 and CuNCs-OCP400, respectively.

Table 1. Total current densities, ECSA-normalized current densities, and ECSA-normalized partial current densities for methane for Cu NCs-OCP200 sample at four potentials.

Potential (V) vs. RHE	J ($mA/cm^2_{geom.}$)	J_{ECSA}(mA/cm^2)	J_{ECSA} [CH_4] (mA/cm^2)
-1.4	**4.020**	**4.129**	**1.108**
-1.3	**2.901**	**3.401**	**0.952**
-1.2	**1.892**	**1.347**	**0.287**
-1.1	**1.166**	**1.515**	**0.059**

Table 2. Total current densities, ECSA-normalized current densities, and ECSA-normalized partial current densities for methane for Cu NCs-OCP400 sample at four potentials.

Potential (V) vs. RHE	J ($mA/cm^2_{geom.}$)	J_{ECSA}(mA/cm^2)	J_{ECSA} [CH_4] (mA/cm^2)
-1.4	**3.908**	**4.621**	**0.101**
-1.3	**2.917**	**1.429**	**0.454**
-1.2	**1.636**	**1.455**	**0.159**
-1.1	**1.197**	**1.370**	**0.143**

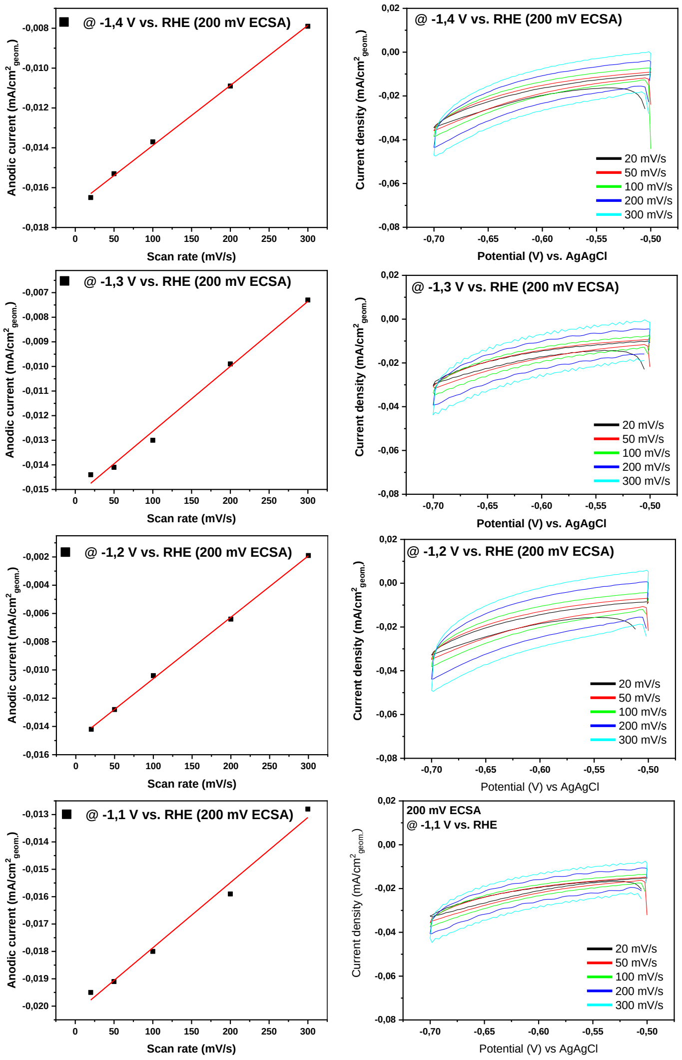

Figure S11. Linear plots of anodic current versus scan rates at the various potentials for Cu NCs-OCP200 sample with the corresponding cyclovoltammograms of 200 mV potential window (-0.7 to -0.5 V vs. Ag/AgCl). The anodic currents were taken at the middle window potential of -0.6 V vs. AgAgCl.

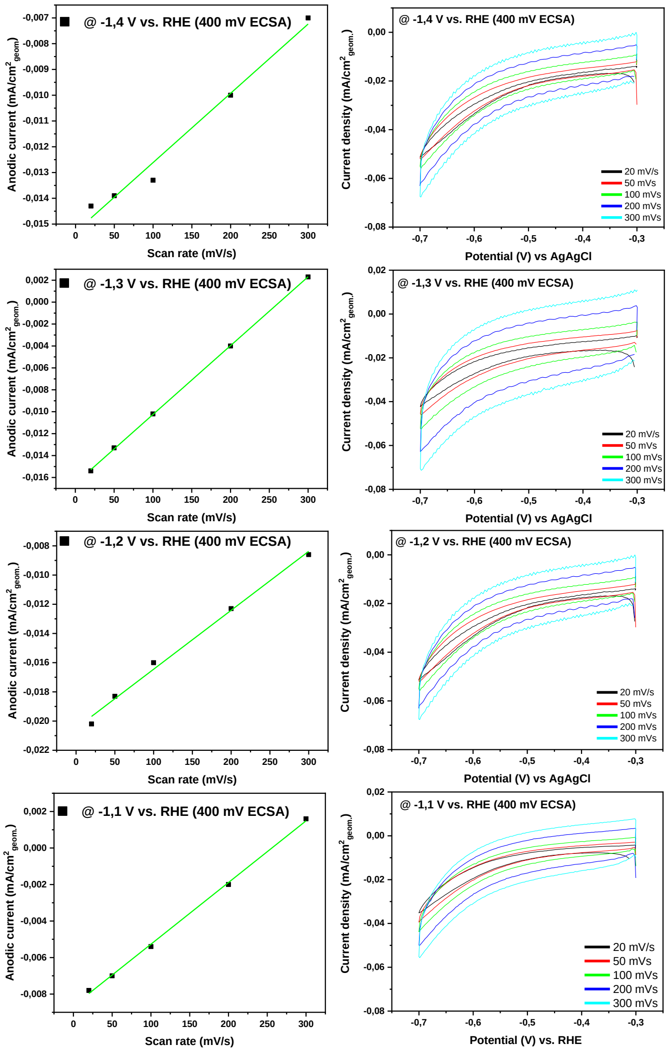

Figure S12. Linear plots of anodic current versus scan rates at the various potentials for Cu NCs-OCP400 sample with the corresponding cyclovoltammograms of 400 mV potential window (-0.7 to -0.3 V vs. Ag/AgCl). The anodic currents were taken at the middle window potential of -0.5 V vs. AgAgCl.

Supplementary note 5

Electrocatalytic measurements

Glassy-carbon plates (Type 2, Alfa Aesar, thickness 3mm) were used as substrates for the working electrode. Before the electrodeposition, they were polished in Milli-Q water slurries of 1.0μm and 0.05μm alumina (Buehler, USA) on a polishing pad with micro cloth (Buehler, USA). The plates were rinsed with Milli-Q water and ultrasonicated in Milli-Q water, acetone, and isopropanol for 10min for each solvent. After sonication, they were blown dry with nitrogen gas. As-synthesized copper nanocubes (Cu NCs) were used as the working electrodes (see Supplementary note 2). Potassium bicarbonate ($KHCO_3$, 99.95% trace metal basis, Honeywell Fluka) was used as the precursor salt for 0.1M electrolyte in CO_2RR measurements. 1.5 ml of 0.1M $KHCO_3$ electrolyte was added to each of the compartments. The electrolyte solution was sparged with CO_2 for at least 30min before CO_2RR experiments. To provide an accurate and constant flow rate, two flow controllers were used for each compartment (Sierra Instruments, Bronkhorst). During electrolysis, CO_2 was constantly bubbled through the electrolyte at a flow rate of 5 sccm to avoid depletion of CO_2 in the electrolyte and to enable a continuous analysis of gaseous products using a gas chromatograph. All electrochemical measurements were done using a dual-channel Biologic SP-300 potentiostat. The electrochemical impedance spectroscopy (EIS) was performed to determine the resistance of the solution and manual iR compensation (85%) was employed during electrolysis in the chronoamperometry regime.

Faradaic efficiency calculations

The gaseous product calculations for Faradaic efficiency were done by the following equation:

$$FE = \frac{n \cdot F \cdot C \cdot G \cdot P}{R \cdot T \cdot I} \quad (equation\ 1)$$

where n is the number of transferred electrons for a particular product (i.e. 2 for CO, 8 for CH_4, etc.), F-Faraday constant (96485 C/mol), C – the measured concentration of the gaseous product by GC (in ppm), G – gas flow rate (in m^3/s), P – pressure (101325 Pa at ambient conditions), R – the universal gas constant (8.314 J/K·mol), T – temperature (293.15 K), I – average cell current after integration of chronoamperometry curve of 1h of reaction (in A).

The liquid product calculation for Faradaic efficiency was done by the following equation:

$$FE = \frac{n \cdot F \cdot C \cdot V}{Q.t} \quad (equation\ 2)$$

where n is the number of transferred electrons for a particular product (i.e. 2 for $HCOO^-$, 6 for methanol, etc.), F-Faraday constant (96485 C/mol), C – the measured concentration of the liquid product by NMR (in mol/dm^3), V – the volume of the separate compartment cathodic or anodic (1.5 ml), Q- total integrated charge for 1h reaction.

Gaseous product detection

The detection of gaseous products was done online by gas chromatography (SRI Instruments #5 GC). Argon 6.0 and hydrogen 5.0 were used as carrier gas and ionization gas, respectively. Figure S11 A shows the connection between the electrochemical reactor and GC. The connection was made through plastic 1/8" tubing (Festo). The CO_2 was constantly purged during electrolysis to avoid depletion of the CO_2 source and the exiting stream was directly inserted into the sampling loop of GC where the expected gaseous products can be identified. The products which are expected are hydrogen (H_2), carbon monoxide (CO), methane (CH_4), ethylene (C_2H_4), and ethane (C_2H_6). The GC (SRI Instruments Multiplegas#5) is equipped with a flame ionization detector (FID) coupled with a methanizer for the detection/quantification of CO and hydrocarbons, and a thermal conductivity detector (TCD) for H_2 detection/quantification (Figure S11 B). The FID detector can detect CO and hydrocarbons down to 1ppm, while the TCD detection limit is less than 100 ppm for H_2. The GC contains a valve oven (2 valves) and a column oven equipped with 3 columns (0.5m and 2m Haysep D column, and 2m Moleseve 5A column). The optimization of GC parameters was done to satisfy both the fast analysis time and the appropriate separation of all products. A temperature of 80 ^{o}C was used for the column oven and 20 psi carrier gas pressure. The variety of opportunities of SRI instruments #5 (2 valves and 3 columns) has enabled us to optimize the analysis method with excellent separation and at the same time fast run with only 8min to elute C_2H_6 (Figure S12A). Calibration of the gas chromatograph was performed using calibration gas standards from Messer. In total 4 calibration standard mixtures were used with 4 different concentrations: (50, 250, 500, 1000) ppm of CO, CH_4, C_2H_4, C_2H_6, and (100, 1000, 5000, 10000) ppm of H_2 balanced in Argon, respectively. The four-point measurement enabled precise calibration for later quantification of unknown concentrations of gaseous products from the CO_2RR reaction (Figure S12 B).

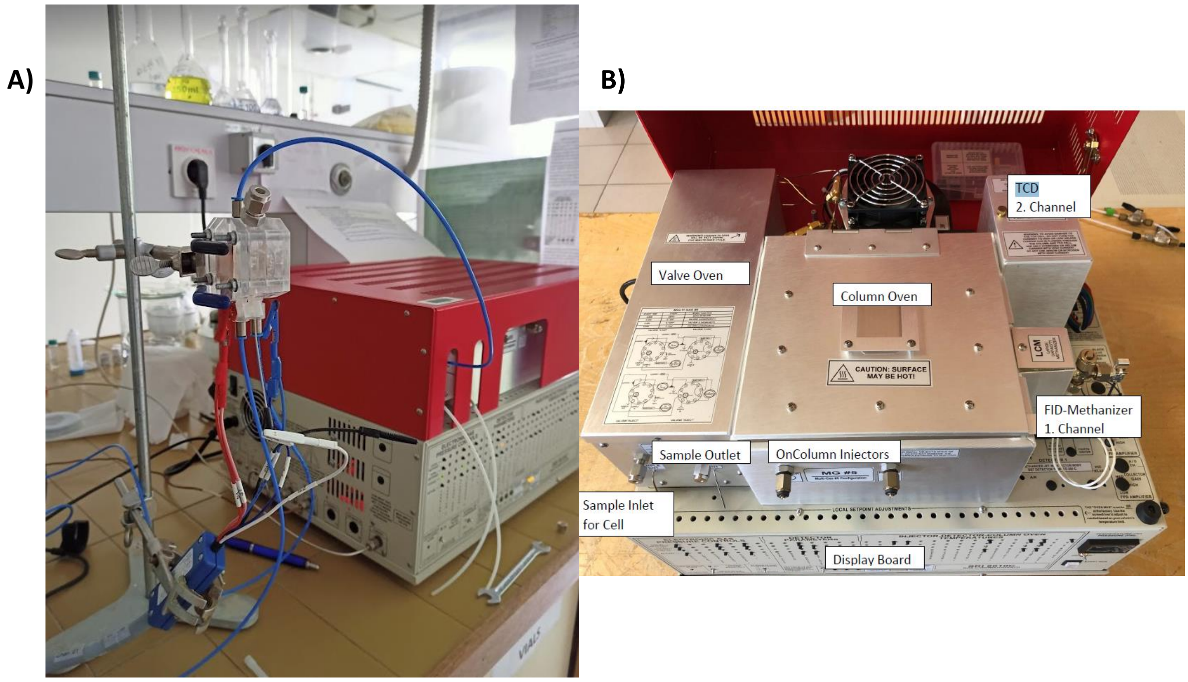

Figure S13. **A)** - Coupled electrochemical sandwich H-type cell and GC for online gaseous product detection. The gas-tight cell with O rings and Festo fittings has enabled continuous measurement of gaseous products without leakage. The injection of the gaseous stream was done every 10 minutes of reaction. **B)** Top-view of the GC (SRI Instruments #5) parts

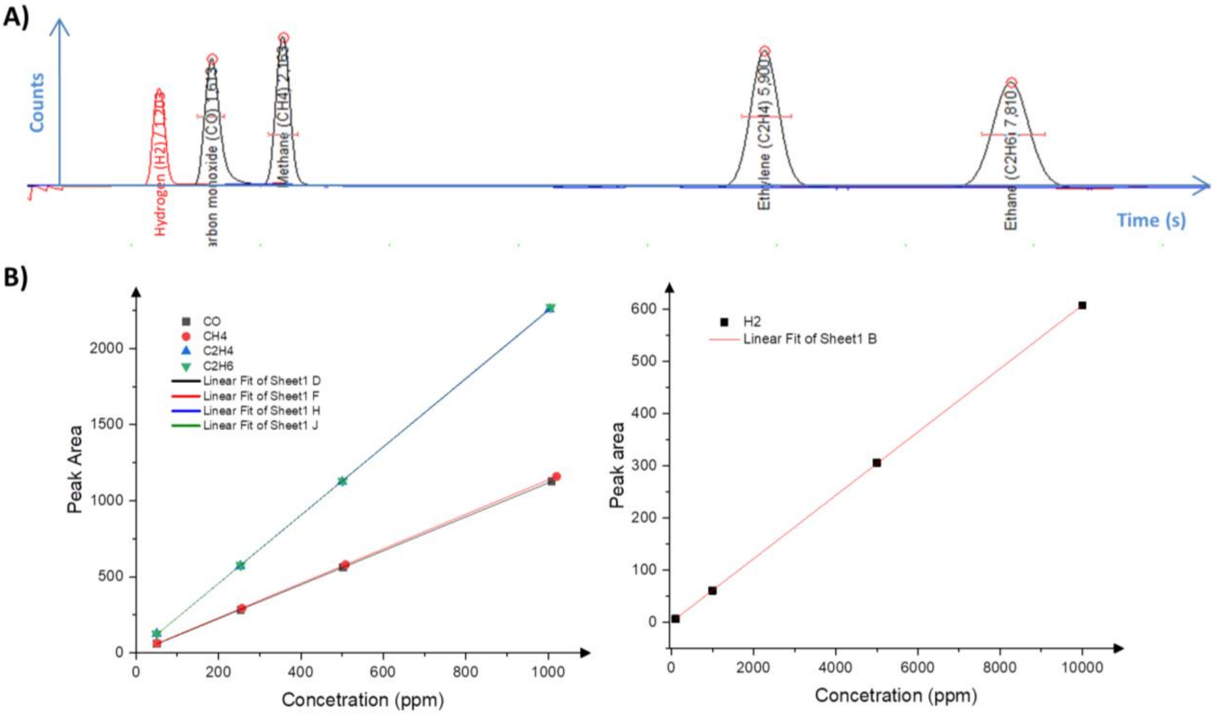

Figure S14. A) FID chromatogram with overlayed TCD signal for H_2 detection (red curve). The FID products elute in the following order: CO, CH4, C_2H_4, and C_2H_6. The good separation was achieved by optimizing the temperature of the column oven and carrier gas pressure. The shown example is for the mixture of 500 ppm (CO, CH_4, C_2H_4, C_2H_6) and 5000 ppm of H_2 balanced in argon. B) Calibration curves for 4 points measurements are shown separately for FID (left) and TCD detected products (right).

The run of one injection was kept for 9,8 min and 0,2 min the delay in-between two injections, which gives 10min of the total time for one GC run. For the usual 1h of reaction time, we had 6 auto sample injections and averaged product concentrations for the calculation of FE (equation 1).

Liquid product detection

Liquid phase products were quantified using 1D ^{1}H NMR experiments recorded on Bruker AVANCE NEO 400 MHz NMR spectrometer equipped with 5 mm BB(F)O Iprobe or BBI probe at 25°C. Noesygppr1d pulse sequence with presaturation during relaxation delay and mixing time was used for suppression of water signal. The spectral width was 7.1 kHz. The repetition delay was 60 s. The number of scans was 16. The obtained 1D ^{1}H NMR spectra were processed and analyzed by Bruker TopSpin software. Potassium phthalate monobasic (KHP) was used as an internal standard for the quantification of products. 1D ^{1}H NMR spectra were referenced on 3-(Trimethylsilyl)propionic-2,2,3,3-d4 acid sodium salt (TMSPA) (δ 0.00 ppm). NMR samples were prepared as follows 540 µL of the electrolyte containing CO_2 reduction products was mixed with 20 µL of D_2O and 40 µL of 0.2 M KHP in D_2O. The final concentration of KHP in 600 µL of NMR samples was thus 20 mM.

Calculation of molar concentration

The signals corresponding to the calibration compound (KHP) were integrated and normalized according to the number of protons giving rise to the signals. The integral values of the products were then compared with those of the calibration compound (KHP). The concentration of a particular product (x) in the presence of a calibrant KHP was calculated using the following formula:

$$C_x = \frac{I_x}{I_{KHP}} \times \frac{N_{KHP}}{N_x} \times C_{KHP} \qquad (equation\ 3)$$

where I, N, and C are the integral area, a number of nuclei (protons that give rise to the signal) and concentration of the product (x), and the calibrant (KHP), respectively.

The identification of signals in 1D ^{1}H NMR spectra corresponding to different liquid phase CO_2 reduction products was based on well-received work by K. Kuhl et al.[9]

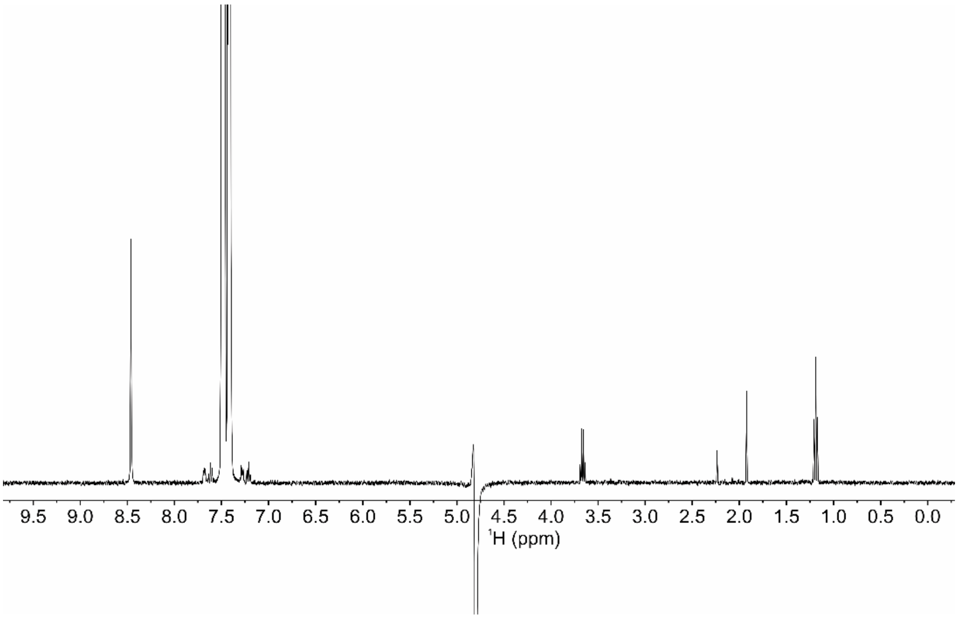

Figure S15. Representative 1D ^{1}H NMR spectrum of liquid phase CO_2 reduction products. The large signals at ca. δ 7.5 ppm correspond to KHP. The signal at δ 8.45 ppm indicates the presence of Formate, quartet, and triplet signals observed at δ 3.66 ppm and δ 1.18 ppm, respectively belong to Ethanol, the signal at δ 2.23 ppm is due to the presence of Acetone, and signal at δ 1.92 ppm belongs to Acetate.

Supplementary note 6

Electrocatalytic performance of as-prepared Cu NCs

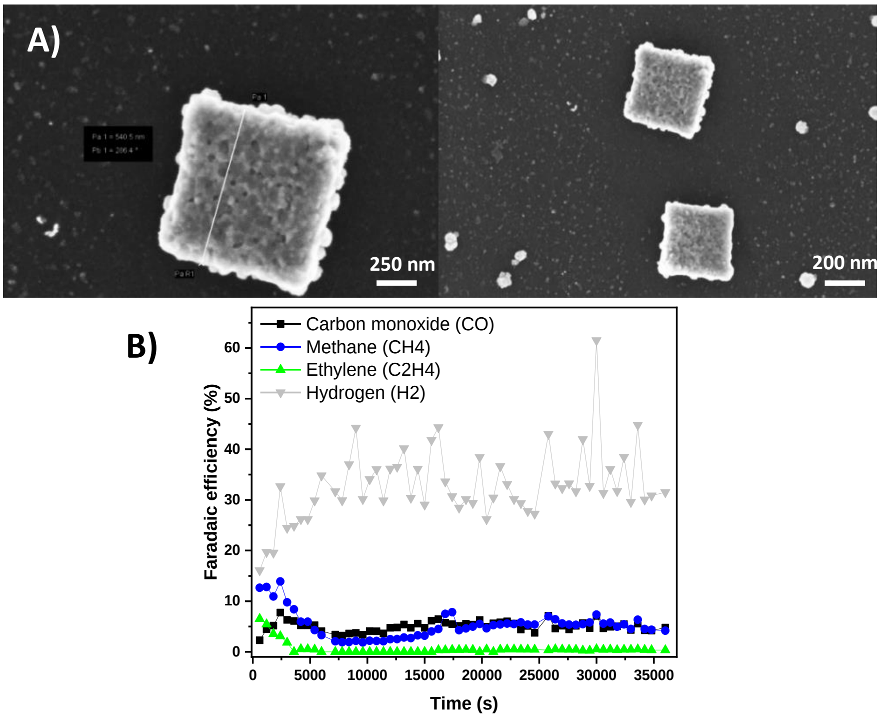

Figure S16. A) Ex-situ SEM images of as-prepared Cu NCs after 1h reaction at -1.3 V vs. RHE which CO$_2$RR inactivity is depicted in Figure 2. B) Time-resolved FE of long-term electrolysis (10h) for as-prepared Cu NCs

Morphological evolution of Cu NCs

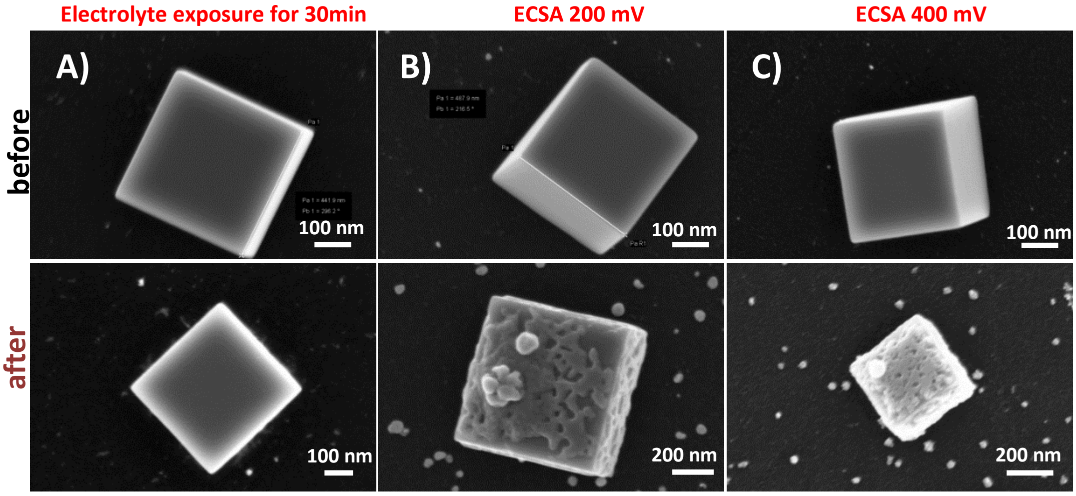

Figure S17. Ex-situ SEM image before and after A) only electrolyte (0.1M KHCO$_3$) exposure of 30 min. There were no significant changes observed in the morphology. B) electrolyte exposure and ECSA treatment in 200 mV potential window (-0.7 to -0.5 V v. AgAgCl) C) electrolyte exposure and ECSA treatment in 400 mV potential window (-0.7 to -0.5 V v. AgAgCl)

Supplementary note 7

Effect of specifically adsorbed chloride anions towards CO chemisorption

Chloride anions are known to affect the electrode kinetics of copper electro-crystallization[10], confirmed the co-adsorption on copper electrodes by *in situ* SERS[11] (surface-enhanced Raman spectroscopy), and also have been reported to alter the double-layer structure.[12] In addition, Lee *et al.*[5] have studied the role of chloride-induced bi-phasic Cu nanostructures in the formation of C_2-C_4 compounds by electrocatalytic CO_2RR. Additionally, the authors emphasize the relative stabilization of Cu^+ states (in Cu_2O) by chloride anions ($Cl^–$).[5,12] As a result, there is an enhancement in the CO chemisorption further leading to C-C coupling. In this context, to understand the role of the selective formation of methane on our Cl^--free Cu NCs, we have explored the CO chemisorption on the Cu_{19} cluster model with and without the presence of Cl^-. This has been investigated with the aid of spin-polarized dispersion-corrected density functional theory-based calculations (More details can be found in ESI-note: Computational details). We have limited our studies only to the model cluster level to distinguish the effects of specifically adsorbed $Cl^–$ and further mechanistic studies on multiple proton-coupled electron transfers to CO and even for C-C coupling is beyond the scope of this work. Here, the main objective is to understand the relative differences on the interaction of CO on copper (particularly using model Cu_{19} cluster) with $Cl^–$ and in the absence of $Cl^–$.

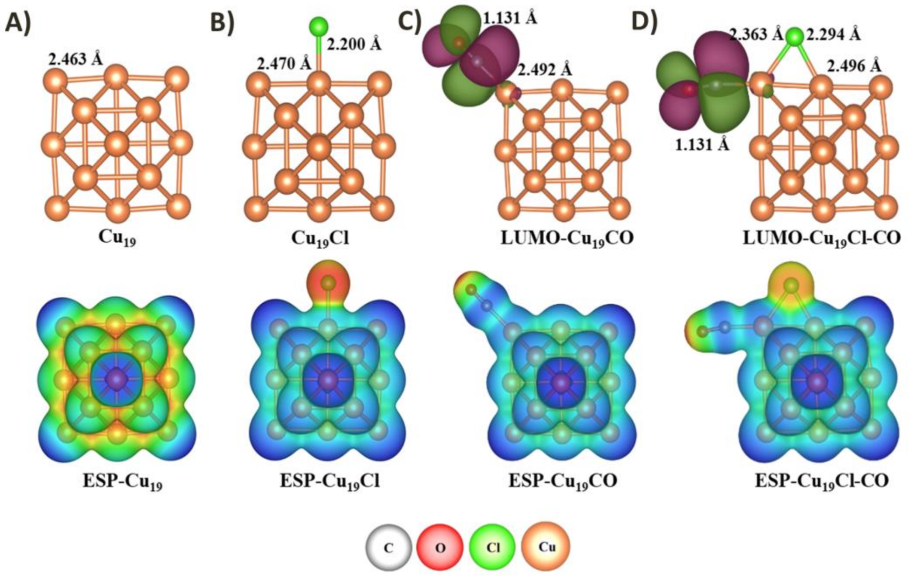

Figure S18. Geometric and electronic properties of Cu_{19} cluster models. A) Cu_{19}; B) $Cu_{19}Cl$; C) $Cu_{19}CO$; D) $Cu_{19}Cl$-CO

Cu-Cu bond lengths in the pristine Cu_{19} cluster model of four nearest neighbor atoms are found to be 2.463 Å and the corresponding electrostatic potential mapping[13] (ESP) is shown in Figure S18 A). ESP is one of the global reactivity descriptors in the finite models (atomic quantum clusters and (macro)molecules), which shed light on the distribution of charges (electron excess/deficiency regions). All the ESPs are plotted with an isosurface value of 0.01 au, where charge distribution regions are relatively color coded with red regions being rich in electron density and the blue color corresponding to low electron density regions. For specifically adsorbed $Cl^–$ on Cu_{19}, the ESP mapping and bond lengths of Cu-Cu and Cu-Cl are shown in Figure S18 B). It is clear from the mapping that specifically adsorbed $Cl^–$ changed the electron density in the very vicinity of Cu atoms (and also relatively of the whole $Cu_{19}Cl$ cluster) due to the inherent electronegativity of halides (region depicted in red). However, there is no noticeable change in the Cu-Cu bond lengths. Nevertheless, copper is known for its affinity toward CO, and chemisorbed CO is the most prominent step for the formation of any hydrocarbons during electrocatalytic CO_2RR. Chemisorbed CO (on $Cu_{19}CO$) with the activated bond length of 1.131 Å and the lowest unoccupied molecular orbital (LUMO-$Cu_{19}CO$) is as represented in Fig1. In this case of $Cu_{19}CO$, ESP mapping looks quite similar to the case of $Cu_{19}Cl$, but with a noticeable change in the Cu-Cu bond length. To understand this change upon CO chemisorption on Cu_{19}, we have calculated atomic charges of nearest neighbor atoms (c.a. four copper atoms around the site of CO adsorption) by natural bond orbital analysis (NBO) methodology. Due to the π-back donation nature of CO, there is a significant charge transfer of -0.42e from CO to bonded copper atom and the adsorption binding energy of -0.94 eV (corrected for basis set superposition errors (BSSE)). Moreover, we have also noticed that there is a symmetric charge (NBO) distribution on the four nearest neighbor copper atoms of CO bonded copper atom. The average charge on these copper atoms is found to be -0.06 e.

Now circumscribing to the specifically adsorbed Cl^- onto CO chemisorbed Cu_{19} cluster, two possibilities where Cl^- can be present in the vicinity of CO have been attempted to understand viz, a case where Cl^- is present on the same copper atom where CO is chemisorbed and the other case where Cl^- is specifically adsorbed on the adjacent copper atom. Both these geometries converged to only one possibility of Cl^- being specifically bound to CO chemisorbed on copper atom (as shown in LUMO- and ESP-$Cu_{19}Cl$-CO, Fig1). In this case, CO bond length activation is similar to the Cl^- free case ($Cu_{19}CO$, Fig1), as well as the Cu-Cu bond lengths, are similar. ESP mapping infers the steric hindrance between these two species and local changes in electron density distribution are only observed. However, NBO charge analysis on CO bonder copper atom infers that there is three times lesser charge transfer (-0.12e) from CO π-back donation. In addition, with the presence of specifically adsorbed Cl^- we find that asymmetric charge distribution on the four nearest neighbor copper atoms of CO-bonded copper atom, and the average charge is found to be -0.15 e. We presume here that this lesser charge transfer is the consequence of more electronegative specifically adsorbed Cl^- in the vicinity of CO and Cu atoms. In addition, these two combined effects of CO chemisorption and specific adsorption of Cl^- have appreciably increased the adsorption binding energy of CO onto copper atoms (-1.20 eV, BSSE correction). This understanding also corroborates the findings on the influence of specifically adsorbing and non-buffering anions like Cl^- towards the formation of hydrocarbons (C2-C4) over copper-based electrocatalysts.[5,14] This specific anion adsorption (S2A) effect plays a direct role in altering the binding energy of important reactive intermediates, influencing the structure of the double layer and interfacial dynamics of charge transfer. Combined studies of theory and experiments on the effect of cations on electrocatalytic CO_2RR has gained momentum in recent years, however similar studies on the influence of anions is sparse in the literature on CO_2RR. This conceptual-DFT-based reactivity descriptor (charge and ESP mapping) study on a simple model copper cluster and from the extensive experimental CO_2RR data over Cl^- free Cu NCs, shed few fundamental and advanced understandings on the selective formation of methane. More rigorous investigations are needed with modeling, theory, experiments, and operando studies are needed in tandem to probe fully the interfacial dynamics of electrocatalytic interfaces.

Computational details:

All the structures presented in this work have been fully optimized with spin-polarized, dispersion-corrected density functional theory-based methodologies as implemented in the Gaussian 16 suite of packages. A hybrid B3LYP (Becke, three-parameter, Lee-Yang-Parr) exchange-correlation functional have been employed in all the calculations; wherein for the atoms C, Cl, and O, Dunning's correlation consistent basis sets with triple zeta valence polarization (cc-pVTZ) basis sets have been used and LANL2DZ (Los Alamos effective core potentials plus with double zeta) effective core potentials have been utilized for the copper atoms. Further, Berny algorithm and extra quadratically convergent (XQC) self-consistent field (SCF) method is used for all the ground state (GS) geometry optimizations. All the optimized GS structures are confirmed as the local minima with all positive vibrational frequencies from the simulated infrared spectra. Charge density and electrostatic potential mapping (ESP) calculations have been performed with the natural atomic orbital and natural bond orbital analysis (NBO) program of Gaussian NBO Version 3.1. The implicit solvation method of SMD (with water as a solvent) performs reaction field calculation using the integral equation formalism model of polarizable conductor calculation (IEFPCM) with radii and non-electrostatic terms. Images of all the optimized geometries are plotted with the aid of VESTA 3.5.5.

References

[1] L.P. Bicelli, B. Bozzini, C. Mele, L. D'Urzo, A review of nanostructural aspects of metal electrodeposition, Int. J. Electrochem. Sci. 3 (2008) 356–408.

[2] P. Grosse, A. Yoon, C. Rettenmaier, S.W. Chee, B.R. Cuenya, Growth Dynamics and Processes Governing the Stability of Electrodeposited Size-Controlled Cubic Cu Catalysts, J. Phys. Chem. C. 124 (2020) 26908–26915. doi:10.1021/acs.jpcc.0c09105.

[3] J.M. Lee, S.H. Lee, Y.J. Kim, J.S. Ko, Effect of the diffusion rate of the copper ions on the co-electrodeposition of copper and nickel, Int. J. Precis. Eng. Manuf. 14 (2013) 2009–2014. doi:10.1007/s12541-013-0273-x.

[4] M.Y. Kazuo Kondo, Rohan N. Akolkar, Dale P. Barkey, Copper Electrodeposition for Nanofabrication of Electronics Devices, 2014. https://books.google.at/books?id=Ge23BAAAQBAJ&pg=PA27&lpg=PA27&dq=10.1007/978-1-4614-9176-7_2&source=bl&ots=up4WV7H85P&sig=soFW7ZJARcXlYsDzFaZ0MreHZhc&hl=en&sa=X&ei=0_bDVJfsDIfVywOA54HYAw&ved=0CCkQ6AEwAg#v=onepage&q=10.1007/978-1-4614-9176-7_2&f=false.

[5] S. Lee, D. Kim, J. Lee, Electrocatalytic Production of C3-C4 Compounds by Conversion of CO 2 on a Chloride-Induced Bi-Phasic Cu 2 O-Cu Catalyst , Angew. Chemie. 127 (2015) 14914–14918. doi:10.1002/ange.201505730.

[6] P. Lobaccaro, M.R. Singh, E.L. Clark, Y. Kwon, A.T. Bell, J.W. Ager, Effects of temperature and gas-liquid mass transfer on the operation of small electrochemical cells for the quantitative evaluation of CO2 reduction electrocatalysts, Phys. Chem. Chem. Phys. (2016). doi:10.1039/c6cp05287h.

[7] C. Wei, S. Sun, D. Mandler, X. Wang, S.Z. Qiao, Z.J. Xu, Approaches for measuring the surface areas of metal oxide electrocatalysts for determining their intrinsic electrocatalytic activity, Chem. Soc. Rev. 48 (2019) 2518–2534. doi:10.1039/c8cs00848e.

[8] M. Lukaszewski, M. Soszko, A. Czerwiński, Electrochemical methods of real surface area determination of noble metal electrodes - an overview, Int. J. Electrochem. Sci. 11 (2016) 4442–4469. doi:10.20964/2016.06.71.

[9] K.P. Kuhl, E.R. Cave, D.N. Abram, T.F. Jaramillo, New insights into the electrochemical reduction of carbon dioxide on metallic copper surfaces, Energy Environ. Sci. 5 (2012) 7050–7059. doi:10.1039/c2ee21234j.

[10] E. Chassaing, Epttaxial Growth and Electrode Impedance, Electrochim. Acta. (1984) 649–660.

[11] G.M. Brown, G.A. Hope, Confirmation of thiourea/chloride ion co-adsorption at a copper electrode by in situ SERS spectroscopy, J. Electroanal. Chem. 413 (1996) 153–160. doi:10.1016/0022-0728(96)04618-9.

[12] W. Shao, G. Pattanaik, G. Zangari, Influence of Chloride Anions on the Mechanism of Copper Electrodeposition from Acidic Sulfate Electrolytes, J. Electrochem. Soc. 154 (2007) D201. doi:10.1149/1.2434682.

[13] P.K. Weiner, R. Langridge, J.M. Blaney, R. Schaefer, P.A. Kollman, Electrostatic potential molecular surfaces, Proc. Natl. Acad. Sci. U. S. A. 79 (1982) 3754–3758. doi:10.1073/pnas.79.12.3754.

[14] Y. Hori, A. Murata, R. Takahashi, Formation of hydrocarbons in the electrochemical reduction of carbon dioxide at a copper electrode in aqueous solution, J. Chem. Soc. Faraday Trans. 1 Phys. Chem. Condens. Phases. 85 (1989) 2309–2326. doi:10.1039/F19898502309.